Atmos. Chem. Phys. Discuss., 8, 15291–15341, 2008
www.atmos-chem-phys-discuss.net/8/15291/2008/

Atmospheric Chemistry and Physics Discussions

This discussion paper is/has been under review for the journal *Atmospheric Chemistry and Physics (ACP)*. Please refer to the corresponding final paper in *ACP* if available.

Cloud and aerosol effects on radiation in deep convective clouds: comparison with warm stratiform clouds

S. S. Lee[1,*], **L. J. Donner**[1], **and V. T. J. Phillips**[1,**]

[1]Geophysical Fluid Dynamics Laboratory, Princeton University, Princeton, NJ, USA
[*]now at: Department of Atmospheric, Oceanic, and Space Science, University of Michigan, Ann Arbor, MI, USA
[**]now at: Department of Meteorology, University of Hawaii, Manoa, HI, USA

Received: 27 May 2008 – Accepted: 15 July 2008 – Published: 12 August 2008

Correspondence to: S. S. Lee (seoungl@umich.edu)

Published by Copernicus Publications on behalf of the European Geosciences Union.

Abstract

Cloud and aerosol effects on radiation in two contrasting cloud types, a deep convective mesoscale cloud ensemble (MCE) and warm stratocumulus clouds, are simulated and compared. At the top of the atmosphere, 45–81% of shortwave cloud forcing (SCF) is offset by longwave cloud forcing (LCF) in the MCE, whereas warm stratiform clouds show the offset of less than ~20%. 28% of increased negative SCF is offset by increased LCF with increasing aerosols in the MCE at the top of the atmosphere. However, the stratiform clouds show the offset of just around 2–5%. Ice clouds as well as liquid clouds play an important role in the larger offset in the MCE. Hence, this study indicates effects of deep convective clouds on radiation and responses of deep convective clouds to aerosols are quite different from those of shallow clouds through the different modulation of longwave radiation; the presence of ice clouds in deep convective clouds contributes to the different modulation of longwave radiation significantly. Different cloud types, characterized by cloud depth and cloud-top height, play critical roles in those different modulations of LCF between the MCE and stratocumulus clouds. Lower cloud-top height and cloud depth lead to smaller offset of SCF by LCF and offset of increased negative SCF by increased LCF at high aerosol in stratocumulus clouds than in the MCE. Supplementary simulations show this dependence of modulation of LCF on cloud depth and cloud-top height is not limited to those two contrasting cloud types. The dependence is also simulated among different types of convective clouds, indicating the assessment of effects of varying cloud types on radiation due to climate changes can be critical to better prediction of climate.

1 Introduction

Among the many atmospheric processes that play a role in climate, clouds are among the most important and difficult to understand. Clouds affect the climate by regulating the flow of radiation at the top of the atmosphere. This regulation process is com-

ACPD

8, 15291–15341, 2008

plicated by cloud microphysics involving numerous processes among different types of hydrometeors such as droplets, ice crystals, rain, snow and hail. This has been a cause of large uncertainties in the prediction of climate changes. Also, increasing aerosols with industrialization are known to change cloud microphysics. Increasing aerosols decrease droplet size and increase cloud albedo (first aerosol indirect effect) and possibly suppress precipitation and alter cloud lifetime (second aerosol indirect effect). Uncertainties of radiative forcing associated with aerosol indirect effects are comparable to radiative forcing by an anthropogenic increase in green house gases (Ramaswamy et al., 2001).

Ramanathan et al. (1989) indicated radiaitve properties of deep convective clouds were different from those of stratiform clouds, regarding the modulation of outgoing longwave radiation. Also, recent studies showed aerosols could change microphysical and dynamical properties of deep convective clouds (Khain et al., 2003, 2004, 2005, 2008; Lynn et al., 2005; Tao et al., 2007; Lee et al., 2008a). Lee et al. (2008b) found aerosol effects on cloud mass and precipitation were different for deep convective and shallow stratiform clouds. Due to stronger interactions between microphysics and dynamics, increases in cloud mass were much larger in deep convective clouds than in shallow stratiform clouds for the same aerosol increases. This indicates the response of radiation to aerosol increases can also be different for deep convective and stratiform clouds.

So far, general-circulation model (GCM) studies have mainly focused on the representation of cloud and aerosol effects on radiation in warm stratiform clouds. Cloud and aerosol effects on radiation in deep convective clouds have not been represented as explicitly as stratiform clouds. In GCM studies, stratiform clouds are represented by microphysics parameterization. However, deep convective clouds are considered sub-grid clouds and, thus, represented by cumulus parameterization. Cumulus parameterizations are unable to simulate cloud dynamics and microphysics explicitly. Thus, cumulus parameterization is not able to consider effects of microphysics on radiation and aerosol effects on dynamics, microphysics and thus cloud mass (both cloud liq-

uid and cloud ice) of deep convection explicitly. Hence, the role of microphysics and aerosols in radiative budget in deep convection has not been represented in a physically realistic way in GCM studies. However, stratiform clouds are considered to be resolved by GCM grids and thus represented more explicitly via microphysics parameterization than deep convective clouds. This enables the simulation of changes in the properties of stratiform clouds caused by green house gases and aerosols in a more realistic way as compared to that in sub-grid deep convective clouds. Hence, GCM studies evaluate the variation of cloud radiative forcing due to green house gases and aerosols mostly based on the variation of cloud radiative forcing of stratiform clouds.

Systems like the Asian and Indian Monsoon, storm tracks, and the intertropical convergence zone (ITCZ), playing important roles in global hydrologic and energy circulations, are driven by deep convective clouds, often organized into mesoscale cloud ensembles (MCEs). Detrainment of ice crystals from the deep convective clouds is the major source of ice anvils and cirrus in these systems. These cirrus clouds have significant impacts on the global radiation budget (Ramanathan et al., 1989; Liou, 2005), and their radiative properties are mainly determined by ice-crystal formation and growth in deep convective clouds (Houze, 1993). Hence, aerosol effects on deep convective clouds can alter radiative properties of cirrus clouds and, thereby, global radiation budget. Especially those systems located over or near continents can be affected by aerosol changes significantly. Hence, the evaluation of variation of cloud radiative forcing due to green house gases and aerosols is needed to be based on changing radiative properties of deep convective clouds as well as changing radiative properties of stratiform clouds for the better prediction of climate changes; the accurate representation of cloud and aerosol effects on radiation in deep convective clouds in GCMs can be critical to the prediction of climate changes. Therefore, it is important to gain the understanding of how deep convective clouds (and their ice clouds) affect radiation and aerosols modify the effects of deep convective clouds on radiation. This contributes to better understanding of cloud and aerosol effects on climate, which can be used to improve the representation of those effects in GCMs. Also, the different cloud effects

on radiation and aerosol effects on cloud radiative properties between deep convective clouds and warm stratiform clouds (suggested in Ramanathan et al., 1989 and Lee et al., 2008b) are needed to be examined. Different cloud and aerosol effects on radiation between deep convective clouds and warm stratiform clouds imply the dependence of those effects on cloud types. This examination will enable us to identify mechanisms of different cloud and aerosol effects on radiation in deep convection as compared to those in warm shallow clouds, which have garnered much more attention than deep convective clouds in climate studies. Identification of mechanisms of different cloud and aerosol effects on radiation between these two contrasting cloud systems enables us to elucidate factors controlling the dependence of those effects on cloud types. This can provide an insight into a more general relation between cloud and aerosol effects on radiation and other types of cloud beyond those two contrasting cloud types.

This study aims to fulfill the following goals: 1) Gain a preliminary understanding of how clouds and aerosols affect radiation in deep convection in a physically realistic way by simulating cloud dynamics and microphysics and their interactions with aerosols explicitly. 2) Examine how those cloud and aerosol effects in deep convection operate differently as compared to warm stratiform clouds to find factors controlling the dependence of those effects on cloud types. To fulfill these goals, cases of a stratocumulus cloud system and an observed deep convective MCE are simulated using a cloud-system-resolving model (CSRM) coupled with double-moment microphysics. The double-moment microphysics predicts cloud particle (i.e., cloud liquid and cloud ice) number as well as cloud particle mass. Nucleation is calculated by considering aerosol number, chemical composition and size distribution. This is different from previous bulk schemes coupled with saturation adjustment or empirical nucleation schemes where initial cloud particles are diagnosed with no consideration of aerosols (See Appendix A for the description of the CSRM). Also, homogeneous aerosol (haze particles) and droplet freezing are considered by using size distribution of unactivated aerosols and taking into account evaporation of small droplets during homogeneous freezing, following Phillips et al. (2007). Hence, it is expected that cloud and aerosol effects

on radiation in deep convection and stratiform clouds are simulated with better confidence in the CSRM adopted here than that in previous bulk schemes coupled with saturation adjustment or empirical nucleation schemes. Impacts of the MCE on radiation and aerosol effects on radiation in the MCE are analyzed and compared to cloud and aerosol effects on radiation in warm marine stratiform clouds. This elucidates processes through which clouds and aerosols affect radiation in deep convective clouds and how they operate differently from those in warm shallow clouds. Those marine stratiform clouds are simulated using the CSRM with smaller domain and finer resolution as compared to those for the simulation of the MCE. This study also examines how ice clouds in the MCE play a role in radiation. To better isolate the different role of clouds and aerosols in radiation, differences in environmental conditions between those two types of clouds needs to be minimized. For this, those two types of clouds are simulated for the same LST (local solar time) period at the same latitude on the same date. Hence, the nearly same incident solar radiation is applied to those two types of clouds. Also, calculations described in the following Sect. 3.1 show the difference in surface longwave radiation flux between two types of clouds is within ~5% relative to the flux in deep convective MCE. Thus, both types of clouds are affected by similar radiation input from the top of the atmosphere (TOA) and the surface.

The simulated MCE was driven using observations from the Atmospheric Radiation Measurement (ARM) Program Southern Great Plains (SGP) summer 1997 intensive operational period (IOP) sub-case A. The simulated stratiform clouds were driven using the reanalysis data from European Centre for Medium-Range Weather Forecast (ECMWF) over the North Atlantic in summer 2002. Two experiments are conducted for each case using the Weather Research and Forecasting (WRF) model as CSRM. The first experiment uses predicted aerosol profiles from Geophysical Fluid Dynamics Laboratory (GFDL) Global Atmosphere Model (AM2) with aerosol chemistry (nudged to analyzed fields) and is referred to as “high-aerosol run”. The second experiment, referred to as “low-aerosol run”, uses aerosol profiles where aerosol mass is reduced by a factor of 10 as compared to the high-aerosol run. Aerosols in the high-aerosol run

for the MCE case represent clean-continental aerosols which are typical in the ARM site and those in the low-aerosol run maritime aerosols. Hence, the comparison of the high- and low-aerosol runs identifies how a transition from maritime aerosols to rather polluted continental aerosols affect radiation. Aerosols in high-aerosol run for the case of marine stratiform clouds showed similar aerosol concentration at the surface to that for the case of the MCE. This is because those stratiform clouds are simulated in near-coastal regions just off the coast of Virginia where significant increases in aerosols advected from the continent were observed since industrialization. Hence, the comparison of the high- and low-aerosol runs for the case of stratiform clouds identifies aerosol effects for the similar transition of aerosol levels to that for the case of the MCE. This indicates the MCE and stratiform clouds both are affected by similar aerosol environment, minimizing differences in aerosol level to contribute to the better isolation of the role of different cloud and aerosol effects on radiation between two types of clouds.

Conclusions only from two contrasting types of clouds can be too limited to establish a generality of mechanisms leading to the variation of cloud and aerosol effects on radiation with varying cloud types. Hence, it is needed to examine cloud and aerosol effects in other types of clouds for the establishment of generality. For this, two additional sets of simulations of different types of convective clouds are performed in an idealized framework. These convective clouds hold an intermediate position between the MCE and stratiform clouds in terms of updraft intensity. Hence, it is expected that these additional idealized simulations can show intermediate cloud and aerosol effects on radiation between those in the MCE and stratiform clouds. This enables not only the better understanding of conclusions from the study of two contrasting types of clouds but also the extension of those conclusions to more types of clouds to contribute to the establishment of the generality.

Integration design and aerosol descriptions are presented in Sect. 2. The results and summary and discussion are given in Sects. 3 and 4.

ACPD
8, 15291–15341, 2008

2 Integration design and aerosol specification

Model domain has 2 dimensions. A mesoscale cloud system typically produces precipitation over areas ∼100 km or more in horizontal scale in at least one direction (Houze, 1993). Hence, for the simulation of the MCE, the horizontal model domain is 168 km and the vertical domain is 20 km to cover a mesoscale system. The horizontal grid length is 2 km, and the vertical grid length is 500 m. Donner et al. (1999) reported a series of test calculations with a similar cloud-system model with resolutions ranging from 500 m to 5 km. They found basic features of the integrations (e.g., patterns of vertical velocity of deep convective cells) were similar for horizontal resolutions of 2 km or finer. For shallower clouds, though, this resolution becomes problematic due to small-scale entrainment and detrainment processes at cloud top, which play important roles in the evolution of shallow stratiform clouds. Hence, finer resolution is used for the simulation of stratiform clouds but with smaller domain to reduce computational burden. The horizontal model domain is 26 km and the vertical domain is 20 km. The horizontal grid length is set to 100 m and the vertical spacing is uniformly 40 m below 2.0 km and then stretched to 240 m near the model top. Periodic boundary conditions are set on horizontal boundaries and a damping layer of 5 km depth is applied near the model top for simulations of both the MCE and stratiform clouds. Henceforth, the MCE and stratiform-cloud cases are referred to as “DEEP” and “SHALLOW”, respectively.

ARM sub-case A (13:30 UTC 29 June–13:30 UTC 30 June 1997) observations provide large-scale forcing for DEEP. Sub-case A produced the largest precipitation rate among the 1997 IOP sub-cases through the development of a deep convective MCE. Sounding/profiler data were obtained every 3hr from the ARM SGP clouds and radiation testbed (CART) central facility located near Lamont, OK (36.61° N, 97.49° W) and from four boundary facilities. They were analyzed using a constrained variational objective analysis method by Zhang et al. (2001). The 3-hourly analyses were used to interpolate large-scale advection for potential temperature and specific humidity at every time step. Observed surface fluxes of heat and moisture were also prescribed. For

ACPD
8, 15291–15341, 2008

SHALLOW, reanalysis data obtained every 6hr from ECMWF at (36.61° N, 74.99° W) (12:00 UTC 29 June–12:00 UTC 30 June 2002) were used to prescribe large-scale forcings and surface fluxes at every time step. Hence, clouds in DEEP and SHALLOW develop at the same LST period and latitude on the same date. The details of the procedure for applying large-scale forcing are described in Donner et al. (1999) and are similar to the method proposed by Grabowski et al. (1996). Horizontal momentum was damped to observed values, following Xu et al. (2002).

The aerosol profiles for these simulations were extracted from a version of the GFDL AM2 (2004) nudged by NCEP reanalysis with aerosol chemistry, since the 1997 ARM observations and the 2002 ECMWF reanalysis do not provide aerosol data. The details of the procedure for nudging the NCEP reanalysis are similar to Timmreck and Schulz (2004). Aerosol chemistry is adopted from Chin et al. (2002) and Koch et al. (1998). Chemical reactions include DMS oxidation by OH during the day and by NO_3 during the night to form SO_2, and SO_2 oxidation by OH in the gas phase and by H_2O_2 in the aqueous phase to form sulfate. The predicted mass profiles, averaged over a one-day period, are obtained at (36.61° N, 97.49° W) on 29 June 1997 and (36.61° N, 74.99° W) on 29 June 2002 for DEEP and SHALLOW, respectively. Vertical profiles of the obtained aerosol, shown in Figures 1a and 1c, are used for the high-aerosol run for DEEP and SHALLOW, respectively. Sulfate, organic and salt aerosols are assumed to act only as cloud condensation nuclei (CCN) and to have tri-modal lognormal size distributions. The mode diameter and standard deviation of the distributions, as well as the partitioning among modes, are assumed to follow Whitby's (1978) values for clean continental air mass and not to vary spatiotemporally for both DEEP and SHALLOW. SHALLOW over the ocean adopts the same mode diameter, standard deviation and partitioning among modes of aerosol distributions as DEEP over the continent, since clouds in SHALLOW are in near-coastal regions just off the coast of Virginia where aerosols advected from the continent are likely to be dominant. Dust and BC aerosols are assumed to act only as ice nuclei (IN) with uni-modal lognormal size distributions. For BC and dust, mode diameter and standard deviation are from Seinfeld and Pan-

ACPD
8, 15291–15341, 2008

dis's (1998) values for remote continental areas. As assumed for aerosols acting as CCN, mode diameter and standard deviation are assumed not to vary for those acting as IN. Aerosol number concentration in each bin of the size spectrum is determined based on aerosol mass and aerosol particle density for each species using the assumed log-normal size distribution at each grid point. Figures 1b and 1d show the vertical profile of the sum of aerosol number concentration over all aerosol species and the CCN number concentration at a supersaturation of 1% for DEEP and SHALLOW, respectively. Total aerosol number concentration at the surface is ~4000 cm^{-3} for DEEP, a typical value in clean continental areas (Whitby, 1978), and ~50% of aerosols are activated at a supersaturation of 1%. For SHALLOW, total aerosol number concentration at the surface is ~3600 cm^{-3} and ~53% of aerosols are activated at a supersaturation of 1%. The low-aerosol runs are conducted with aerosol profiles obtained by reducing aerosol masses used for high-aerosol run by a factor of 10. Hence, the surface aerosol number concentration is ~400 cm^{-3} in the low-aerosol runs, a typical value in maritime air, not affected by pollution (Whitby, 1978). Depending on predicted aerosol mass within cloud, the total aerosol number for each aerosol species varies and is reset to the background value at all levels outside cloud. Within clouds, aerosols are advected, diffused and depleted by nucleation. Initially aerosol mass mixing ratio is everywhere set equal to its background value. Background aerosol number concentrations for all aerosol species in each aerosol size mode are assumed not to vary during time integration, since the variation of the extracted aerosols from GFDL AM2 is not significant on the date of simulations.

This study focuses on aerosol effects on cloud radiative properties and, thus, does not take into account aerosol direct effects on radiation.

ACPD
8, 15291–15341, 2008

3 Results

3.1 Radiation fluxes

The all- and clear-sky radiative fluxes for shortwave and longwave radiation are obtained. The clear-sky fluxes are diagnosed by setting the mixing ratios of all the hydrometeors to zero with all the other variables unchanged at every time step for the high- and low-aerosol runs, respectively. Henceforth, the clear-sky condition is referred to as "CLR" and the all-sky as "ALL". Radiation fluxes are shown in Tables 1 and 2 for DEEP and SHALLOW, respectively (↑ and ↓ denote upward and downward fluxes, respectively, and minus signs indicate downward net flux). In Tables, SW and LW represent shortwave flux and longwave flux, respectively. Table 3 shows SCF, LCF, and cloud radiative forcing (CRF), which is SCF+LCF, in DEEP and SHALLOW. Cloud forcing here is defined as CLR − ALL. The role of ice clouds in DEEP is diagnosed by setting the mixing ratio of all ice-phase hydrometeors to zero with all the other variables unchanged at every time step for the high- and low-aerosol runs. Henceforth, this ice-free condition is referred to as "DEEP (LIQ)" and cloud forcing in DEEP (LIQ) is presented in Table 3. The comparison of DEEP (LIQ) to DEEP identifies the role of ice clouds in radiation.

Differences in individual upward and downward fluxes between the high-aerosol run and observation in DEEP are within ∼10% relative to observed fluxes, demonstrating clouds in DEEP are simulated reasonably well. Since ECMWF data do not provide observed fluxes, simulated liquid-water path (LWP) and effective diameter in SHALLOW are compared to observation by the Moderate Resolution Imaging Spectroradiometer (MODIS) to assess ability of the model to simulate stratiform clouds. The domain-averaged simulated LWP is 56.20 g m^{-2} and MODIS-observed LWP at the location of simulation is 59.35 g m^{-2}. In-cloud average effective size of simulated cloud liquid is 18.56 μm and MODIS-observed size is 17.10 μm. Hence, differences are within ∼10%, demonstrating clouds in SHALLOW are also reasonably well simulated.

SCF is counterbalanced substantially more by LCF at the top of the atmosphere in

ACPD
8, 15291–15341, 2008

each high- and low-aerosol runs in DEEP than in SHALLOW (Table 3). At the top of the atmosphere, 45% (81%) of SCF is counterbalanced by LCF in the high-aerosol run (low-aerosol run) in DEEP. However, in SHALLOW, just 13% (16%) of SCF is counterbalanced in the high-aerosol run (low-aerosol run). At the bottom of the atmosphere, differences in the counterbalance between DEEP and SHALLOW are negligible as compared to those at the top. Larger counterbalance in deep convective clouds than in shallow stratiform clouds at the top of the atmosphere is also observed by Ramanathan et al. (1989). They found that SCF was substantially counterbalanced by the reduction of outgoing LW in deep convective regions mainly associated with Aisan and Indian Monsoon, storm tracks and ITCZ. However, their data indicated the counterbalance in the regions of stratiform clouds was not as strong as in deep convective regions.

The high-aerosol run shows larger negative SCF by 23.85 and 18.22 $W\,m^{-2}$ than the low-aerosol run at the top in DEEP and SHALLOW, respectively (Table 3). This is mainly because more SW is reflected in the high-aerosol run than in the low-aerosol run by 23.72 $W\,m^{-2}$ and 18.10 $W\,m^{-2}$ in DEEP and SHALLOW, respectively, as shown in Tables 1 and 2. Since clouds in the high-aerosol run decrease the outgoing LW more than in the low-aerosol run in both DEEP and SHALLOW (Tables 1 and 2), LCF is larger in the high-aerosol run than in the low-aerosol run by 6.52 W m^{-2} and 0.45 W m^{-2} in DEEP and SHALLOW, respectively, at the top (Table 3). Similar to the larger compensation of SCF by LCF in each low- and high-aerosol runs in DEEP than in SHALLOW at the top, the variation of SCF due to aerosol changes is offset by that of LCF much more in DEEP than in SHALLOW. 28% of an increase of negative SCF due to aerosol increases is offset by that of LCF in DEEP, whereas SHALLOW shows the offset of just 2% at the top. DEEP shows significantly larger offset than SHALLOW for changing SCF and LCF with increasing aerosols at the bottom as well as at the top. 19% (2%) of the increase in negative SCF is offset by the increase in LCF in DEEP (SHALLOW) at the bottom of the atmosphere.

In the absence of ice clouds in DEEP (LIQ), the offset of SCF by LCF is reduced to 42% (25%) in the high-aerosol run (the low-aerosol run) as compared to those in the

ACPD
8, 15291–15341, 2008

presence of ice clouds (DEEP) at the top (Table 3). However, still, the offset in each high-aerosol run and low-aerosol run in DEEP (LIQ) is larger than in SHALLOW. The offset of increased negative SCF by increased LCF with increasing aerosols is also reduced to 18% in the absence of ice clouds at the top in DEEP (LIQ). However, the offset in DEEP (LIQ) is also still larger than that in SHALLOW.

SCF at both high and low aerosols is much more substantially offset by LCF in DEEP than in SHALLOW at the top. This indicates that deep convective clouds affect the radiation budget quite differently as compared to stratiform clouds in terms of the modulation of LW. Results here also indicate that the aerosol-induced modulation of LW can substantially offset that of SW in deep convective clouds, which has not been considered in most GCM studies. To gain understanding of these different responses of radiation between deep convective and shallow clouds, the effective size and mass of hydrometeors, which determine the radiative properties of clouds, are examined.

3.2 Radiative properties of clouds

Figure 2a–c show the profiles of effective size, and Fig. 3a–c, the profiles of the contents of cloud liquid, cloud ice, and rain in DEEP. Since graupel is treated radiatively in the same manner as for snow in DEEP, they are treated as one hydrometeor entity, referred to as "snow+graupel," and the vertical profile of the sum is depicted in Fig. 3d. The effective size of snow+graupel is prescribed as 150 μm for both runs in DEEP. The vertical profiles of effective size and contents of cloud liquid in SHALLOW are presented in Figures 2d and 3e, respectively. Note that stratiform clouds in SHALLOW are warm clouds where ice processes are not present with negligible precipitation. Average precipitation rate is smaller than 0.01 mm day^{-1} in both the high- and low-aerosol runs. Hence, only size and mass of cloud liquid are presented for SHALLOW. The contribution of rain and snow+graupel to radiation budgets is negligible as compared to that of cloud liquid and cloud ice in DEEP, because their particle sizes are generally larger than the radiation wavelengths. Hence, this study focuses on the role of cloud liquid and cloud ice in radiation among hydrometeors. The role of cloud liquid, accounting for

larger fraction of total cloud-particle (cloud liquid and cloud ice) mass than cloud ice and all cloud mass in DEEP and SHALLOW (see Fig. 3a, b and e), respectively, in radiation are first examined. Time- and domain-average liquid-water content (LWC) is 0.0025 (0.0020) and 0.0006 (0.0013) g m^{-3} in the high- and low-aerosol runs, respectively, in DEEP (SHALLOW). Although in-cloud average LWC is larger in DEEP than in SHALLOW, domain-average LWC is lower at low aerosol due to lower cloud fraction in DEEP than in SHALLOW. Averaged cloud fractions over whole simulation period and a layer between minimum cloud-base height and maximum cloud-top height at low aerosol in DEEP and SHALLOW are 0.27 and 0.90, respectively. Also, the domain-average difference in LWC at high aerosol between DEEP and SHALLOW is smaller than the in-cloud average difference due to lower cloud fraction in DEEP. Averaged cloud fractions at high aerosol in DEEP and SHALLOW are 0.32 and 0.95, respectively. Larger LWC in DEEP than in SHALLOW in the high-aerosol run favors more absorption of LW emitted from the surface, contributing to the larger offset of SCF by LCF in DEEP than in SHALLOW (Table 3). The comparison of DEEP (LIQ) to SHALLOW indicates liquid clouds alone can lead to larger offset of SCF by LCF in deep convective clouds than in warm shallow clouds (Table 3). However, cloud fraction and domain-average LWC are smaller in the low-aerosol run in DEEP than in SHALLOW, favoring more absorption of LW emitted from surface in SHALLOW. In addition to cloud mass and fraction, temperature at the top of liquid cloud affects outgoing LW and the top of liquid cloud is higher in both the high- and low-aerosol runs in DEEP than in SHALLOW (Fig. 3a and e). As shown by Jensen et al. (1994), LCF at the top of the atmosphere is roughly proportional to the difference in temperature between cloud top and the surface for the identical cloud optical depth. As shown in Fig. 3a, liquid-cloud top reaches around 10 km where average temperature is 232 K in DEEP. In SHALLOW, liquid-cloud top reaches just around 1 km (Fig. 3e) where average temperature is 286 K. At the surface, the average temperature is 295 K in DEEP and 288 K in SHALLOW. Hence, larger vertical extent of liquid cloud leading to larger temperature difference between liquid-cloud top and the surface in DEEP than in SHALLOW contributes to larger offset

ACPD
8, 15291–15341, 2008

of SCF by LCF in tandem with increased liquid mass at high aerosol. The effect of this larger temperature difference on LCF outweighs the effect of decreased liquid mass and cloud fraction on LCF, leading to more offset of SCF by LCF in liquid clouds in DEEP than in SHALLOW at low aerosol as can be seen in the comparison between DEEP (LIQ) and SHALLOW.

In addition to LWC, ice-water content (IWC) plays a role in radiation in DEEP, which is absent in SHALLOW. As indicated by Liou (2005), ice clouds play an important role in the trapping of LW from the surface and their high altitude enhances the reduction of outgoing LW. Their higher altitude than that of liquid clouds, as shown in Fig. 3a and b, increases LCF and thereby the offset of SCF by LCF at the top as compared to those when only liquid clouds are considered. The offset of SCF by LCF increases from 25% in DEEP (LIQ) to 45% in DEEP at the top at high aerosol. At low aerosol, the offset increases from 42% to 81% at the top. These indicate ice clouds play as important roles as liquid clouds for larger offset of SCF by LCF in each high- and low-aerosol runs in DEEP than in SHALLOW at the top of the atmosphere.

Significant differences are observed in effective sizes of cloud liquid, liquid content, and ice content between high- and low-aerosol runs in DEEP (Figs. 2a, 3a, and b). The high-aerosol run has higher liquid content and smaller liquid sizes than the low-aerosol run, and the ice content is also larger in the high-aerosol run. Cloud liquid is ~5 times greater around 4 km in the high-aerosol run. Cloud ice content is ~4 times larger at high aerosol around 10 km. Larger cloud water content at high aerosol is due to increased condensation and deposition. Domain-averaged cumulative condensation and deposition is larger in the high-aerosol run than in the low-aerosol run by 25.04 mm and 8.30 mm, respectively. The smaller size of cloud liquid is due to larger cloud droplet number concentration (CDNC) in the high-aerosol run. The high-aerosol run shows 3–5 times larger CDNC below freezing level where most differences in droplet size are observed (Fig. 4a). Time- and domain-average cloud liquid at high aerosol in SHALLOW is larger than that at low aerosol by ~53%, much smaller than ~320% increase shown in the high-aerosol run in DEEP (Fig. 3a and e). In SHALLOW, the

ACPD
8, 15291–15341, 2008

size of cloud liquid is smaller at high aerosol than at low aerosol due to larger CDNC as in DEEP (Fig. 4b). The smaller differences in cloud-liquid content are due to smaller increases in condensation in the high-aerosol run than those in DEEP. Domain-average cumulative condensation increases in the high-aerosol run by ~28%, which is ~7 times smaller increase as compared to that in DEEP.

Larger cloud mass and fraction (note that averaged cloud fractions are 0.32 (0.95) and 0.27 (0.90) at high and low aerosols in DEEP (SHALLOW), respectively), smaller size of cloud particles at high aerosol favor larger reflection and absorption of downward SW (and more outgoing SW at the model top and less SW reaching the surface). Increased cloud mass and fraction at high aerosol also affects LW. More LW emitted from the surface is absorbed by clouds at high aerosol, leading to smaller outgoing LW at the top and larger downward LW at the surface in the high-aerosol run than in the low-aerosol run (Tables 1 and 2). Those changes in LW offset changes in SW and high-aerosol run in DEEP shows larger offset than in SHALLOW mainly due to larger increases in cloud mass (Fig. 3 and Table 3).

It should be pointed out that there are significant increases in cloud-ice content in the high-aerosol run in DEEP, contributing to more reflection and absorption of SW and LW, respectively. The comparison of DEEP to DEEP (LIQ) indicates changes in ice-particle mass affects the offset of increased reflection of SW by increased absorption of LW significantly at high aerosol. DEEP and DEEP (LIQ) show the difference of 27% and 18% in the offset between high- and low-aerosol runs, respectively, at the top of the atmosphere (Table 3). This indicates increased cloud-ice content accounts for about a third of increased offset at high aerosol at the top.

Increased condensation and deposition at high aerosol are due to more updraft activity as shown in Fig. 5 illustrating the updraft mass fluxes in the high- and low-aerosol runs. The increased updraft activity is linked to enhanced near-surface convergence at high aerosol, which in turn results from increased downdrafts driven by evaporation. Delayed autoconversion due to higher CDNC provides more abundant cloud liquid to be transported into unsaturated areas as the source of this increased evaporation.

These feedbacks between dynamics and microphysics are described in more detail in Lee et al. (2008a) and simulated in Khain et al. (2003, 2004, 2005, 2008) and Lynn et al. (2005). Lee et al. (2008b) indicated increases in updrafts, leading to increases in condensation and deposition, were much larger in deep convective clouds than those in shallow clouds at high aerosol as shown in Fig. 5a and b. They found that increased cloud particles were transported to unsaturated areas more efficiently due to stronger convective motion at high aerosol in deep convective clouds than in shallow clouds. Hence, evaporation increase was much larger at high aerosol in deep convective clouds than in shallow clouds. Also, downdrafts with increased intensity from increased evaporation could be accelerated more as they descended to the surface at high aerosol due to deeper cloud depth providing longer path for their descent in deep convective clouds than in shallow clouds. This leads to more enhanced near-surface convergence and updrafts at high aerosol in deep clouds than in shallow clouds.

Maximum CAPE is $\sim$2500 J kg^{-1} and maximum wind shear is $\sim$15 m s^{-1} in DEEP (The wind shear is defined as the difference between density-weighted mean wind speed over the lowest 6 km of the profile and average wind speed over the lowest 500 m of the profile, following Weisman and Klemp, 1982). According to Bluestein (1993), these CAPE and shear conditions support the development of deep cumulonimbus-type clouds, as simulated in DEEP, leading to larger differences in updrafts between the high- and low-aerosol runs than in SHALLOW. Shallow clouds exhibited less detrainment of cloud liquid. The limited vertical extent of shallow clouds reduced differences in evaporative cooling, convergence and updrafts between high and low aerosol cases, leading to smaller increases in condensation and deposition. These account for the smaller offset of increased negative SCF by increased LCF at high aerosol in SHALLOW than in DEEP. The differing responses of deep and shallow clouds to increased aerosol are depicted schematically in Fig. 6.

ACPD
8, 15291–15341, 2008

3.3 Idealized stratiform clouds

Although similar radiation input (at TOA and the surface) and aerosols are applied to both types of clouds in DEEP and SHALLOW, the other environmental factors may have affected differences in cloud and aerosol effects on radiation between DEEP and SHALLOW simulated here. It is ideal to keep the environmental conditions (e.g., initial condition, surface albedo, large-scale forcing and surface fluxes) to be identical for those different types of clouds to better isolate cloud and aerosol effects on radiation. However, it is unlikely to simulate different types of clouds with identical conditions, since Weisman and Klemp (1982) and Bluestein (1993) show strong dependences of cloud types on environmental factors such as CAPE and wind shear. Moreover, warm stratiform clouds develop under neutrally stratified condition in the planetary boundary layer (PBL) with strong inversion on its top while deep convective clouds develop under unstable conditions. Hence, it is needed to find a compromise by simulating different types of clouds while minimizing differences in environmental conditions. To further minimize differences in environmental condition between the MCE and warm stratiform clouds, an idealized simulation of stratiform clouds (henceforth, referred to as SHALLOW (IDEAL)) at the same LST period and location on the same date in the same year as for DEEP is performed. Hence, there are no differences in radiation input at TOA and nearly no differences in radiation input at the surface between DEEP and SHALLOW (IDEAL). Also, there are no differences in background aerosols and surface albedo between DEEP and SHALLOW (IDEAL). To generate the idealized stratiform clouds, the same initial condition, large-scale forcing and surface fluxes as for DEEP are used for SHALLOW (IDEAL) except for larger-scale temperature forcing to contribute to the further minimization of differences in environmental conditions. For SHALLOW (IDEAL), positive large-scale temperature forcing is applied around the freezing-level as shown in Fig. 7b, whereas negative temperature forcing is applied around the freezing-level for DEEP as shown in Fig. 7a. The positive temperature forcing around the freezing-level favors the formation of inversion layer and thus formation of shallow warm stratiform

ACPD
8, 15291–15341, 2008

clouds. This generates stratiform clouds developing under nearly similar environment to that in DEEP. High- and low-aerosol runs for SHALLOW (IDEAL) are performed using the same aerosol profiles as for the high- and low-aerosol runs, respectively, in DEEP. The same domain size and grid horizontal and vertical lengths as in SHALLOW are used for SHALLOW (IDEAL).

Time- and domain-averaged LWC is 0.0030 and 0.0020 g m^{-3} in the high- and low-aerosol runs, respectively, in SHALLOW (IDEAL). Averaged cloud fractions calculated in the same manner as for DEEP and SHALLOW are 0.98 and 0.95 at high and low aerosol, respectively. Although LWC and cloud faction in SHALLOW (IDEAL) are larger than those in DEEP in both the high- and low-aerosol runs, favoring more absorption of LW from the surface in SHALLOW (IDEAL), more fraction of SCF is counterbalanced by LCF in DEEP than in SHALLOW (IDEAL) in both the high- and low-aerosol runs. Just 11% (18%) of SCF is counterbalanced in the high-aerosol run (low-aerosol run) in SHALLOW (IDEAL), whereas 45% (81%) of SCF is counterbalanced by LCF in the high-aerosol run (low-aerosol run) in DEEP at TOA (Tables 3 and 4) (DEEP (CU) and DEEP (LOW-CU) in Table 4 will be described in the following section). This is because cloud-top in SHALLOW (IDEAL) reaches just around 2 km where average temperature is ~293 K. As shown in the previous section, deep convective clouds in DEEP reaches more than 10 km where average temperature is smaller than 232 K. Since average surface temperature is nearly the same (~295 K) in both DEEP and SHALLOW (IDEAL), the difference in temperature between cloud top and the surface is much smaller in SHALLOW (IDEAL) than in DEEP. This leads to much smaller offset of SCF by LCF in SHALLOW (IDEAL) than in DEEP despite larger LWC and cloud fraction. Increasing cloud fraction and mass with varying cloud types from cumulonimbus in DEEP to stratocumulus in SHALLOW (IDEAL) contribute to increases in negative SCF in both the high- and low-aerosol runs. However, due to lowering cloud-top height, LCF decreases with this variation of cloud types in both the high- and low-aerosol runs, leading to the smaller offset of SCF by LCF in SHALLOW (IDEAL) than in DEEP (Tables 3 and 4).

Due to substantially less detrainment of cloud liquid and limited vertical extent of

ACPD
8, 15291–15341, 2008

shallow clouds in SHALLOW (IDEAL), differences in evaporative cooling, convergence and updrafts between high and low aerosol cases reduce as depicted in Fig. 6. Note that cloud top is around 2 km in SHALLOW (IDEAL). This leads to cloud-liquid increase of ~50% in the high-aerosol run, ~6 times smaller increase than that shown in DEEP. This in turn leads to much smaller offset of increased negative SCF by increased LCF in SHALLOW (IDEAL) than that in DEEP. Just 5% of increased negative SCF is offset by increased LCF in SHALLOW (IDEAL), whereas DEEP shows the offset of as much as 28% at TOA. Different cloud depth and convective motion determine the different offset of increased negative SCF by increased LCF with increased aerosols by controlling evaporative cooling and acceleration of descending downdrafts.

Different cloud depth and cloud-top height primarily determine the different offset of SCF by LCF and of increased negative SCF by increased LCF at high aerosol between SHALLOW (IDEAL) and DEEP. It is expected that environmental conditions do not contribute to these different responses of radiation significantly in this study. Analysis here shows that differences in responses of radiation to clouds and aerosols between SHALLOW and DEEP are similar to those between SHALLOW (IDEAL) and DEEP despite different environmental conditions between SHALLOW and SHALLOW (IDEAL). This indicates different responses of radiation between deep clouds and low-level shallow clouds are fairly robust to environmental conditions and cloud-top height and cloud depth play an important role in those different responses.

3.4 Idealized convective clouds

Different modulation of LCF between the deep convective MCE and stratiform clouds is mostly due to differences in cloud depth and cloud-top height. This implies different modulation of LCF even among different types of convective clouds with different cloud depth and cloud-top height. To examine the sensitivity of modulation of LCF to types of convective clouds, two sets of additional simulations of idealized convective clouds are performed. Each set of simulations is composed of the high- and low-aerosol runs.

Updrafts play an important role in cloud depth and cloud-top height of convective

clouds; stronger updrafts carry cloud particles higher. Updraft strength is partly determined by CAPE (Weisman and Klemp, 1982). To generate convective clouds with different cloud-top height and cloud depth, different CAPE levels are applied to those additional sets of simulations. Comparisons among DEEP and these additional simulations elucidate the dependence of the effects of clouds and aerosols on radiation on types of convective clouds. To better isolate this dependence, differences in environmental conditions among three cases of convective clouds in this study need to be minimized. For the minimization, only initial humidity fields and humidity forcing at the lowest level are imposed differently to generate different CAPE levels. This is because CAPE shows strong sensitivity to lowest-level humidity predominantly controlled by surface fluxes. Modification of humidity at the lowest level for the generation of different CAPEs is also used in Lee et al. (2008b). Except for the lowest-level humidity, the identical environment and aerosol conditions and model setup of the high-aerosol run (the low-aerosol run) in DEEP are applied to the high-aerosol run (the low-aerosol run) in these additional simulations of idealized convective clouds. In the first set of simulations, moderate CAPE value of $\sim$1500 J kg^{-1} is applied, which is to support the formation of cumulus clouds according to Bluestein (1993). In the second of set of simulations, low CAPE value of $\sim$500 J kg^{-1} is applied, which is to support the formation of low-level cumulus clouds according to Bluestein (1993). Henceforth, the first and second sets of simulations are referred to as DEEP (CU) and DEEP (LOW-CU), respectively.

Figure 8 depicts the time series of humidity large-scale forcing and area-averaged water vapor mixing ratio at the lowest level of the atmosphere for DEEP, DEEP (CU) and DEEP (LOW-CU). The negative forcing at the lowest level in DEEP (CU) and DEEP (LOW-CU) lowers water vapor at the lowest level by offsetting the strong positive moisture flux at the surface prior to 16:40 UTC on 29 June. The vapor mixing ratio at the lowest level begins to rise around 16:40 UTC when the negative forcing is removed due to the surface moisture flux. Note that identical surface fluxes are prescribed in DEEP, DEEP (CU), and DEEP (LOW-CU). Hence, after the negative forcing is removed, the

ACPD
8, 15291–15341, 2008

mixing ratio in DEEP (CU) and DEEP (LOW-CU) stabilizes to a value lower than that in DEEP around 16:30 UTC (Fig. 8a and b). Due to different humidity levels at the lowest level, the maximum CAPE during simulations is different. The maximum CAPEs are $\sim$1500 J kg^{-1} and $\sim$500 J kg^{-1} for DEEP (CU) and DEEP (LOW-CU), respectively, as intended. The maximum CAPE in DEEP is $\sim$2500 J kg^{-1} where cumulonimbus-type clouds are dominant. With lower CAPE in DEEP (CU) than in DEEP, cumulus-type clouds are as dominant as cumulonimbus-type clouds in DEEP (CU). With the lowest CAPE among three cases of convective clouds, lower cumulus clouds as compared to those in DEEP (CU) are dominant in DEEP (LOW-CU). Lower CAPEs in DEEP (CU) and DEEP (LOW-CU) than in DEEP lead to lower cloud depth and cloud-top height as can be seen in the comparison between Figs. 3 and 9. Figure 9 depicts vertical profiles of time- and domain-averaged cloud liquid and cloud ice content in DEEP (CU) and DEEP (LOW-CU). Due to lower CAPE, clouds in DEEP (LOW-CU) show lower cloud depth and cloud-top height than those in DEEP (CU) (Fig. 9).

Time- and domain-averaged cloud mass (cloud liquid + cloud ice) is 0.0027 (0.0010) and 0.0028 (0.0017) g m^{-3} at high (low) aerosol in DEEP (CU) and DEEP (LOW-CU), respectively. Averaged cloud fractions calculated in the same manner as for DEEP are 0.40 (0.38) and 0.51 (0.50) at high (low) aerosol in DEEP (CU) and DEEP (LOW-CU), respectively. Although LWC and cloud faction in DEEP (CU) and DEEP (LOW-CU) are larger than those in DEEP in both the high- and low-aerosol runs, favoring more absorption of LW from the surface in DEEP (CU) and DEEP (LOW-CU), more fraction of SCF is counterbalanced by LCF in DEEP than in DEEP (CU) and DEEP (LOW-CU) in both the high- and low-aerosol runs. 27% (34%) and 22% (25%) of SCF is counterbalanced in the high-aerosol run (the low-aerosol run) in DEEP (CU) and DEEP (LOW-CU), respectively, whereas 45% (81%) of SCF is counterbalanced by LCF in the high-aerosol run (the low-aerosol run) in DEEP as shown in Tables 3 and 4. This is because cloud-top heights in DEEP (CU) and DEEP (LOW-CU) are lower than those in DEEP as shown in Figs. 3 and 9, leading to smaller differences in temperature between cloud top and the surface. Due to lower cloud-top height, smaller

portion of SCF is counterbalanced by LCF in DEEP (LOW-CU) than in DEEP (CU) (Table 4). Increasing cloud fraction and mass with varying dominant cloud types from cumulonimbus in DEEP to cumulonimbus and cumulus in DEEP (CU) contribute to increases in negative SCF. However, due to lowering cloud-top height, LCF decreases with this variation of cloud types, leading to smaller offset of SCF by LCF in DEEP (CU) than DEEP (Tables 3 and 4). Transition of dominant cloud type from cumulonimbus and cumulus in DEEP (CU) to low-level cumulus in DEEP (LOW-CU) also accompanies increasing cloud fraction and mass, contributing to increases in negative SCF. LCF also increases with this transition at low aerosol. However, due to lowering cloud-top height with this transition, increases in LCF are not as large as in those in negative SCF, leading to smaller offset of SCF by LCF in DEEP (LOW-CU) than in DEEP (CU) at low aerosol (Tables 3 and 4). At high aerosol, with this transition of cloud type, LCF decreases due to lowering cloud-top height, leading to smaller offset of SCF by LCF in DEEP (LOW-CU) than in DEEP (CU) at high aerosol (Tables 3 and 4).

Smaller vertical extent of clouds in DEEP (CU) and DEEP (LOW-CU) than in DEEP leads to smaller differences in evaporative cooling, convergence and updrafts between high and low aerosol cases. Figure 10 shows differences in updrafts are smaller in DEEP (CU) and DEEP (LOW-CU) than in DEEP. This leads to smaller cloud-mass increases at high aerosol in DEEP (CU) and DEEP (LOW-CU) than in DEEP. Increases of cloud-mass at high aerosol are ~170% and 65% in DEEP (CU) and DEEP (LOW-CU), respectively. DEEP (CU) and DEEP (LOW-CU) show ~2 and ~5 times smaller increases than DEEP, respectively. This in turn leads to smaller offset of increased negative SCF by increased LCF at high aerosol in DEEP (CU) and DEEP (LOW-CU) than that in DEEP. 23 (18)% of increased negative SCF is offset by increased LCF in DEEP (CU) (DEEP (LOW-CU)), whereas DEEP shows the offset of as much as 28% at TOA. Also, smaller vertical extent of clouds leads to smaller offset of increased negative SCF by increased LCF at high aerosol in DEEP (LOW-CU) than in DEEP (CU).

Different cloud-top heights play a critical role in different offset of SCF by LCF in each high- and low-aerosol runs among three cases of convective clouds. Different

ACPD
8, 15291–15341, 2008

cloud depths lead to different offset of increasing negative SCF by increasing LCF at high aerosol among three cases of convective clouds.

Simulations for stratiform and convective clouds in this study demonstrate that cloud-top height and cloud depth play a critical role in the offset of SCF by LCF and offset of increasing negative SCF by increasing LCF at high aerosol.

4 Summary and discussion

Cloud and aerosol effects on radiation in a deep convective MCE (DEEP) and warm stratocumulus clouds (SHALLOW) were investigated using double-moment bulk microphysics. Aerosol mass, CDNC, cloud-ice number concentration, and cloud particle size were predicted. For the nucleation of cloud particles, the chemical composition, size spectrum, and number concentration of aerosols were considered.

DEEP showed larger offset of SCF by LCF at the top of the atmosphere than SHALLOW at both high and low aerosol. In SHALLOW, less than 20% of SCF is offset by LCF, whereas, in DEEP, the offset is 45% at high aerosol and as much as 81% at low aerosol. It is notable that ice clouds contributed to the offset as much as liquid clouds in DEEP. When the effect of cloud ice on radiation was excluded, the compensation reduced to 25 (42)% at high (low) aerosol at the top in DEEP. Ramanathan et al. (1989) also found that SCF was substantially counterbalanced by the reduction of outgoing LW in deep convective regions: (i) the tropical Pacific and Indian oceans surrounding Indonesia and the Pacific ITCZ north of the equator; (ii) the monsoon region in Central Africa and the northern third of South America; and (iii) the mid-latitude storm tracks in the Pacific and Atlantic oceans. The counterbalance is most significant in tropical convective regions where the reduction of outgoing LW nearly cancelled SW cloud forcing. They also found cirrus in those regions provided a significant contribution to the reduction of outgoing LW as diagnosed here. However, the reduction of outgoing LW relative to increases in outgoing SW due to clouds in the regions of stratiform clouds is not as significant as in deep convective regions. Hence, their study indicates deep

ACPD
8, 15291–15341, 2008

convective clouds affect radiation quite differently in terms of the modulation of LW as compared to shallow stratus- or stratocumulus-type clouds as simulated in this study. An additional idealized simulation of warm stratiform clouds (SHALLOW (IDEAL)) with the nearly same environmental conditions as in those in DEEP was carried out. This was to better isolate mechanisms leading to differences in cloud and aerosol effects on radiation between deep convective clouds and warm stratiform clouds. This simulation showed that differences in cloud-top height played a critical role in differences in the offset of SCF by LCF between deep convective clouds and warm stratiform clouds. This dependence of the relative magnitude of LCF to SCF on cloud-top height indicates changing environmental conditions due to climate changes may impact global offset of SCF by LCF as briefly mentioned in Ramanathan et al. (1989). As an example, increases in temperature around the Earth's surface due to increases in green house gases can change the surface humidity, and, thereby, CAPE. As indicated in Weisman and Klemp (1982) and Bluestein (1993) and simulated in DEEP (CU) and DEEP (LOW-CU), CAPE plays an important role in the determination of cloud-top height. This is because CAPE basically determines the intensity of updrafts. Low CAPE generally leads to low updrafts, reducing vertical transport of hydrometeors and, thus, cloud-top height. This relation between CAPE and cloud-top height was simulated in Lee et al. (2008b). Lee et al. (2008b) showed the transition of the cloud type from high-level cumulonimbus to low-level cumulus to warm stratiform clouds with decreasing CAPE caused by decreasing surface humidity. According to Clausius-Clapeyron equation, saturation water-vapor pressure increases exponentially with increasing temperature. Hence, the increasing surface temperature due to green house gases can increase surface humidity. This increases CAPE. Thus, it is expected that the offset of SCF by LCF can be larger with increasing green house gases based on the comparisons of radiation among DEEP, DEEP (CU), and DEEP (LOW-CU) where CAPE levels varied. The evaluation of this changing offset can be critical to assess the response of climate to green house gases, considering the strong sensitivity of the offset to cloud-top height shown in the comparison study of convective clouds and stratiform clouds simulated

here.

Increases in negative SCF due to aerosol increases were found to be offset by increases in LCF more significantly in deep convective clouds than in warm shallow clouds. This was mainly due to larger increases in cloud mass (both in liquid and ice water) in deep convective clouds than in shallow clouds. Stronger feedbacks between dynamics and microphysics led to larger increases in cloud mass in deep convection than in shallow clouds as described in Lee et al. (2008b). SHALLOW and SHALLOW (IDEAL) showed that shallower cloud depth led to less intense feedbacks between dynamics and microphysics by providing shorter path to the surface for descending downdrafts in warm stratiform clouds than in deep convective clouds. Hence, different cloud depth played a critical role in different offset of increased negative SCF by increased LCF at high aerosol between deep convective clouds and warm shallow clouds. Even among the convective clouds with different cloud depth, the offset of increased negative SCF by increased LCF at high aerosol was different. As the cloud type changed from cumulonimbus (DEEP) to cumulonimbus and cumulus (DEEP (CU)) to low-level cumulus (DEEP (LOW-CU)), cloud depth decreased (Figs. 3 and 9). This led to decreasing offset of increased negative SCF by increased LCF at high aerosol. The offset was the smallest in stratiform clouds among simulations of convective clouds and stratiform clouds due to the smallest cloud depth of stratiform clouds. These indicate the critical role the cloud depth plays in aerosol-induced cloud mass and LCF changes.

Cirrus clouds regularly cover 20–25% of the globe and as much as 70% over the tropics and, thus, can act as one of major modulators of global radiation budget (Liou, 1986, 2005). Houze (1993) indicates that most cirriform cloud is of the type that has its origin in the upper layers of deep, precipitation cloud systems. Ice clouds played as important roles as liquid clouds in the offset of SCF by LCF in clouds in DEEP. Large increases in ice mass with increasing aerosols in deep convective clouds simulated here implies subsequent increases in cirrus clouds detrained from parent deep convective clouds. Hence, this study suggests the feedback in deep convective clouds depicted in Fig. 6 can have a significant impact on global radiation budget by modi-

ACPD
8, 15291–15341, 2008

fying thickness and coverage of cirrus clouds. Increasing ice clouds simulated here accounted for ~30% of the offset of increased negative SCF by increased LCF with increasing aerosols in DEEP. Thus, increasing cirrus clouds with increasing aerosols can enhance this so-called infrared warming effects, though its global impact will depend on the relationship between aerosol distribution and deep convection, a matter this study was not able to consider. So far, most GCMs have not taken into account homogeneous freezing of droplets and haze particles for sub-grid convective clouds, playing important roles in development of ice clouds in deep convective systems, explicitly. Also, most GCMs have mostly focused on low-level stratiform clouds for the evaluation of changes in cloud radiative forcing by aerosol increases. They have not taken into account aerosol effects on deep convection or the links of these effects on detrained cirrus. These may contribute to the large uncertainties associated with the effects of ice clouds on radiation and aerosol indirect effects, considering the significant warming effect by ice clouds shown here.

Generally, sub-grid convective clouds in climate models have been represented by cumulus parameterization which is not able to simulate microphysics explicitly. Hence, it is hard to expect that varying modulation of LCF with varying cloud-top height in convective clouds has been reasonably simulated in climate models. This is because cloud-top height is determined by the upward transportation of hydrometeors by updrafts and microphysical properties of hydrometeors affect the transportation significantly. Those properties of hydrometeors affect microphysical processes such as nucleation, phase transition and collision having a substantial impact on latent heat distribution, cloud particle and precipitation mass, which, in turn, affect the intensity of updrafts. Also, it is hard to expect that the important roles ice clouds, associated with microphysical processes such as heterogeneous and homogeneous nucleation, play in the modulation of LCF have been reasonably simulated in climate models. Moreover, cumulus parameterization is not able to represent aerosol-induced intense interactions between microphysics and dynamics in convective clouds playing an important role in the offset of increasing negative SCF by increasing LCF with increas-

ing aerosols. Considering that increasing green house gases can lead to changes in cloud-top height and increasing aerosols can modify aerosol-induced interactions between microphysics and dynamics and thus the property of ice clouds in convective cloud systems, more accurate and explicit representation of convective clouds in climate models is needed to better predict climate changes.

This study demonstrates that different cloud and aerosol effects on radiation among different types of clouds were strongly controlled by cloud vertical extent and cloud-top height. The larger cloud-top height of clouds was the primary cause of large LCF, leading to the larger offset of SCF by LCF in deeper clouds. Also, the larger vertical extent of deeper clouds enabled much more intense low-level downdrafts, leading to substantially increased updrafts and cloud mass at high aerosol as compared to those in comparatively shallower clouds. This led to more offset of increased negative SCF by increased LCF at high aerosol in deeper clouds. Hence, experiments here suggest that cloud- and aerosol-induced infrared warming effects primarily depend on the cloud-top height and cloud depth. However, this does not exclude the possibility of impacts of environmental conditions on those infrared warming effects. Even in similar types of clouds with similar cloud-top height and cloud depth, slightly different environmental conditions such as humidity and large-scale subsidence above the PBL, sea surface temperature (SST), and surface sensible and latent heat fluxes can change cloud development and aerosol-cloud interactions (Jiang et al., 2002; Ackerman et al., 2004; Guo et al., 2007; Khain et al., 2008). Hence, more case studies of various types of clouds under various environmental conditions are needed to address those impacts of environmental conditions and to better establish the generality of results here in future studies.

Acknowledgements. The authors wish to thank Venkatachalam Ramaswamy for valuable discussions. Our thanks also go to Paul Ginoux for the review of the manuscript and Charles Seman for providing us useful post-processors. This paper was prepared under award NA17RJ2612 from the National Oceanic and Atmospheric Administration, US Department of Commerce. The statements, findings, conclusions, and recommendations are those of authors and do not necessarily reflect the views of the National Oceanic and Atmospheric Administra-

tion, or the US Department of Commnerce.

Appendix A

Description of cloud-system-resolving model

A1 Dynamics, turbulence, and radiation

For numerical experiments, the Weather Research and Forecasting (WRF) model (Michalakes et al., 2001) is used as a two-dimensional nonhydrostatic compressible model. The detailed equations of the dynamical core of WRF are described by Klemp et al. (2000).

Hong and Pan's (1996) scheme, which includes non-gradient flux for heat and moisture and calculates vertical eddy diffusion, is used for the PBL. For vertical diffusion in the free troposphere, Hong et al.'s (2006) scheme, where diffusion is represented with an implicit local scheme based on the local Richardson number, is used. The version of WRF used in these experiments uses a turbulence kinetic energy (TKE) closure. Horizontal eddy diffusion is a function of TKE, following Chen and Dudhia (2000).

For radiation, a simplified version of the GFDL radiation code is incorporated into WRF (Freidenreich and Ramaswamy, 1999; Schwarzkopf and Ramaswamy, 1999). The radiative effects of cloud liquid, cloud ice, rain, snow, graupel, water vapor, CO_2, and O_3 are included. Effective sizes of cloud liquid and cloud ice are predicted using assumed size distributions. A generalized effective size of cloud ice is inferred from the mean size of the equivalent spherical diameter following Phillips et al. (2007).

A2 Double-moment microphysics

To represent microphysical processes, the WRF is modified to use Phillips et al.'s (2007) double-moment bulk representation. The size distribution of cloud liquid

and cloud ice (x=c, i) obeys a gamma distribution:

$$n(D_x) = n_{x,0} D_x^{p_x} \exp[-\lambda_x D_x] \quad \text{(A1)}$$

where D_x is the equivalent spherical diameter (m) and $n(D_x)dD_x$ is the number concentration (m^{-3}) of particles in the size range dD_x. Also, λ_x (m^{-1}) is the slope, $n_{x,0}$ is the intercept ($m^{-(4+p_x)}$), and p_x is the shape parameter of the distribution.

$\lambda_x = \left(\frac{\Gamma(4+p_x)\rho_x \frac{\pi}{6} n_x}{\Gamma(1+p_x) q_x}\right)^{\frac{1}{3}}$ and $n_{x,0}=(n_x \rho_a)\lambda_x^{1+p_x}/\Gamma(1+p_x)$. Here, Γ is the Gamma function, ρ_x and n_x are the particle bulk density ($kg\,m^{-3}$) and number mixing ratio (kg^{-1}) (particle number per unit air mass), respectively. ρ_a is the air density. For ice particles, a bulk density close to that of pure solid-column ice crystal is assumed (ρ_i=900 $kg\,m^{-3}$) (Young, 1993). The general conclusions obtained in this study also hold if different bulk density of ice particles is used. However, the shape dependence of ice crystals on temperature and humidity has not been taken into account, and this could alter riming in the calculations. $p_i$and p_c are set to unity and 3.5, respectively, based on field experiments described in Phillips et al. (2007). Further description of the bulk microphysics can be found in Phillips et al. (2007).

A3 Droplet nucleation

Droplet nucleation follows Ming et al.'s (2006) nucleation parameterization. In their parameterization, aerosol can take any form of size distribution and chemical composition. Critical supersaturation (S_c) and critical radius (r_c) are calculated considering aerosol chemical composition, based on the Köhler theory. For surface tension depression by dissolved organic substances, Facchini et al's (1999) measured suppression is used. Maximum supersaturation (S_{max}) of a closed adiabatic parcel is calculated based on the equation of supersaturation prediction from Leaitch et al. (1986) for primary nucleation, occurring in cloud-free air; the supersaturation in the parcel increases with increasing vertical positive velocity of updrafts and decreases with increasing condensation. When the increase exactly counterbalances the decrease, the supersaturation

ACPD
8, 15291–15341, 2008

is at its equilibrium $S_{\max}$. $S_{\max}$ is obtained by solving Leaitch et al.'s equation of supersaturation prediction numerically. $S_{\max}$for secondary nucleation (in-cloud nucleation) is obtained from Phillips et al.'s (2007) linearized supersaturation scheme. Aerosols, whose S_c is lower than S_{max}, are counted as nucleated droplets in Ming et al.'s (2006) parameterization.

A4 Ice nucleation

Lohmann and Diehl's (2006) parameterizations, taking into account the dependence of IN activation on dust and BC on aerosol mass, are used for contact, immersion, and condensation-freezing activation of IN. For contact activation:

$$\frac{dN_{\mathrm{CNT}}}{dt}(m^{-3}s^{-1}) = m_{io}D_{ap}4\pi r_{cm}N_{a,\mathrm{cnt}}\frac{\rho_a n_c^2}{q_c} \quad \text{(A2)}$$

where $\frac{dN_{\mathrm{CNT}}}{dt}$ is the rate of ice-crystal number production via contact freezing, m_{io} (10^{-12} kg) is the original mass of a newly formed ice crystal, D_{ap} ($\mathrm{m^2\,s^{-1}}$) is the Brownian aerosol diffusivity, r_{cm} is volume-mean droplet radius, $N_{a,\mathrm{cnt}}$ ($\mathrm{m^{-3}}$) is the number concentration of contact nuclei and n_c is the number mixing ratio of droplets. D_{ap} is given by

$$D_{ap} = \frac{kTC_c}{6\pi\eta r_m}$$

where k is the Boltzmann constant, T is the temperature, η is the viscosity of air $\{\eta=10^{-5}\ (1.718+0.0049(T-T_0)-1.2\times10^{-5}(T-T_0)^2)$ in $\mathrm{kg\,m^{-1}\,s^{-1}}\}$, r_m is the aerosol mode radius, and C_c is the Cunningham correction factor $[C_c=1+1.26(\frac{\lambda}{r_m})(\frac{p_0}{p})(\frac{T}{T_0})]$. The aerosol mode radius is taken to be 0.2 μm for dust and 0.1 μm for BC. λ is the molecular free path length of air (λ=0.066 μm), p_0 and T_0 refer to standard pressure of 1013.25 hPa and freezing temperature of 273.16 K. $N_{a,\mathrm{cnt}}$ is obtained from the number

of aerosol particles consisting of BC and dust, multiplied by a temperature dependence of the individual species. This temperature dependence is based on Fig. 1 in Lohmann and Diehl (2006). Here, for dust, temperature dependence of montmorillonite is adopted (Lohmann and Diehl, 2006). For immersion and condensation-freezing activation:

$$\frac{dN_{\mathrm{IMM}}}{dt}(m^{-3}s^{-1}) = N_{a,\mathrm{imm}} \exp(T_0 - T)\frac{dT}{dt}\frac{\rho_a q_c}{\rho_c} \quad \text{(A3)}$$

where $\frac{dN_{\mathrm{IMM}}}{dt}$ is the rate of ice-crystal number production via immersion and condensation freezing, T_0 freezing temperature. $N_{a,\mathrm{imm}}$ (m^{-3}) is the number concentration of immersion and condensation nuclei calculated as the number of BC and dust aerosols, multiplied by a temperature dependence for immersion and condensation freezing in Fig. 1 in Lohmann and Diehl (2006). ρ_c is the water density. As for contact freezing, temperature dependence of montmorillonite is adopted for dust. For deposition nucleation, Möhler et al.'s (2006) parameterization, calculating the fraction of dust activated, is implemented:

$$\frac{dN_{\mathrm{DEP}}}{dt}(m^{-3}s^{-1}) = N_{a,\mathrm{dep}}(\exp[a(S_i - S_0)] - 1) \quad \text{(A4)}$$

where $\frac{dN_{\mathrm{DEP}}}{dt}$ is the rate of ice-crystal number production via depositional freezing, a and S_0 are non-dimensional empirical constants determined by chamber experiments. Here a and S_0 are set to 4.77 and 1.07, respectively, based on experiments for desert dust. $N_{a,\mathrm{dep}}$ is the number concentration of deposition nuclei (m^{-3}) calculated from predicted total dust mass. Eq. (A4) is applied at temperatures colder than –40°C and restricted to $S_0 < S_i < 1.63 + 6.52 \times 10^{-3} \times (T - T_0)$, corresponding to Field et al.'s (2006) measured saturation region where pure deposition nucleation occurs. The parameterization is limited to activating a maximum of 5% of the dust, following Field et al.'s (2006) measurements. As indicated by Field et al.'s (2006) experiments, (A4) is only valid at temperatures below –40°C. At temperatures warmer than –40°C, Meyer et al. (1992)

ACPD
8, 15291–15341, 2008

and DeMott et al.'s (2003) parameterizations, multiplied by a scaling factor to consider the dependence of IN activation on dust mass, are used. For temperatures between –30 and –40°C:

$$N_{IN}(m^{-3}) = 1000(\exp[12.96(S_i - 1.1)])^{0.3} \times \Psi \quad \text{(A5)}$$

Here, N_{IN} is ice-crystal number concentration, S_i the saturation ratio with respect to ice and Ψ a scaling factor to take into account the dependence of IN activation on dust mass. Ψ is $\frac{DU_{2.5}}{DU^*_{2.5}}$, where $DU_{2.5}$ is mass concentration of dust particles with diameter less than 2.5 μm and $DU^*_{2.5}$ is the average dust mass concentration. $DU^*_{2.5}$ is set at 0.11 $\mu g\,m^{-3}$ based on dust data from the Mount Werner project used to derive Eq. (A5) (DeMott et al., 2003). Hence, Eq. (A5) computes N_{IN} based on variation of dust mass relative to an average level of dust mass observed at the Mount Werner project. It was observed that IN concentrations were almost linear with the concentrations of large aerosol particles (Berezinskiy et al., 1986; Georgii and Kleinjung, 1967). Hence, it is a good assumption N_{IN} is proportional to $DU_{2.5}$. For temperatures between –5 and –30°C, the same scaling factor as used in Eq. (A5) is applied to Meyers et al.'s (1992) parameterization as follows, since dust mass data are not available in Meyers et al. (1992):

$$N_{IN}(m^{-3}) = 63\exp[12.96(S_i - 1) - 0.639] \times \Psi \quad \text{(A6)}$$

Equations (A5) and (A6) are applied to grid points with no cloud liquid to ensure only deposition nucleation is calculated. They are limited to activating a maximum of 0.5% of the dust, since Field et al. (2006) found deposition nucleation did not activate more than 0.5% of the dust at temperatures warmer than –40°C.

References

Ackerman, A. S., Kirkpatrick, M. P., Stevens, D. E., and Toon, O. B.: The impact of humidity above stratiform clouds on indirect aerosol climate forcing, Nature, 432, 1014–1017, 2004.

Bluestein, H. B.: Synoptic-Dynamic Meteorology in Midlatitudes: Volume II: Observations and Theory of Weather Systems (Synoptic-Dynamic Meteorology in Midlatitudes), Oxford University Press, 594 pp., 1993.
Berezinskiy, N. A., Stepanov, G. V., and Khorguani, V. G.: Altitude variation of relative ice-forming activity of natural aerosol, S. Meterol. Hydr., 12, 86–89, 1986.
Chin, M., Ginoux, P., Kinne, S., et al.: Tropospheric Aerosol Optical Thickness from the GOCART Model and Comparisons with Satellite and Sun Photometer Measurements, J. Atmos. Sci., 59, 441–460, 2002.
Chen, S.-H. and Dudhia, J.: Anuual report: WRF physics, Air Force Weather Agency, 38 pp., 2000.
DeMott, P. J., Cziczo, D. J., Prenni, A. J., Murphy, D. M., Kreidenweis, S. M., Thomson, D. S., Borys, R., and Rogers, D. C.: Measurements of the concentration and composition of nuclei for cirrus formation, Proc. Natl. Acad. Sci. USA, 100, 25, 14 655–14 660, 2003.
Donner, L. J., Seman, C. J., and Hemler, R. S.:Three-dimensional cloud-system modeling of GATE convection, J. Atmos. Sci., 56, 1885–1912, 1999.
Facchini, M. C., Mircea, M., Fuzzi, S., and Charlson, R. J.: Cloud albedo enhancement by surface-active organic solutes in growing droplets, Nature, 401, 257–259, 1999.
Field, P. R., Möhler, O., Connolly, P., Krämer, M., Cotton, R., Heymsfield, A. J., Saathoff, H., and Schnaiter, M.: Some ice nucleation characteristics of Asian and Saharan desert dust, Atmos. Chem. Phys., 6, 2991–3006, 2006, http://www.atmos-chem-phys.net/6/2991/2006/.
Freidenreich, S. M. and Ramaswamy, V.: A new multiple-band solar radiative parameterization for general circulation models, J. Geophys. Res., 104, 31 389–31 410, 1999.
Georgii, H. W. and Kleinjung, E.: Relations between the chemical composition of atmospheric aerosol particles and the concentration of natural ice nuclei, J. Rech. Atmos., 3, 145–146, 1967.
Grabowski, W. W., Wu, X., and Moncrieff, M. W.: Cloud resolving modeling of tropical cloud systems during phase III of GATE. Part I: Two-Dimensional Experiments, J. Atmos. Sci., 53, 3684–3709, 1996.
Guo, H., Penner, J. E., Herzog, M., and Xie, S.: Investigation of the first and second aerosol indirect effects using data from the May 2003 Intensive Operational Period at the Southern Great Plains, J. Geophys. Res., 112, D15206, doi:10.1029/2006JD007173, 2007.
Hong, S.-Y. and Pan, H.-L.: Nonlocal boundary layer vertical diffusion in a medium range fore-

cast model, Mon. Wea. Rev., 124, 2322–2339, 1996.
Hong, S.-Y, Noh, Y., and Dudhia, J.: A New Vertical Diffusion Package with an Explicit Treatment of Entrainment Processes, J. Atmos.Sci., 24, 2318–2341, 2006.
Houze, R. A.: Cloud dynamics, Academic Press, 573 pp., 1993.
Jensen, E. J., Kinne, S., and Toon, O. B.: Tropical cirrus cloud radiative forcing: Sensitivity studies, Geophys. Res. Lett., 18, 2023–2026, 1994.
Jiang, H., Feingold, G., and Cotton, W. R., Simulations of aerosol-cloud-dynamical feedbacks resulting from entrainment of aerosol into the marine boundary layer during the Atlantic Stratocumulus Transition Experiment, J. Geophys. Res., 107, 4813, doi:10.1029/2001JD001502, 2002.
Khain, A., and Pokrovsky, A.: Simulation of Effects of Atmospheric Aerosols on Deep Turbulent Convective Clouds Using a Spectral Microphysics Mixed-Phase Cumulus Cloud Model, Part II: Sensitivity Study, J. Atmos.Sci., 24, 2983–3001, 2004.
Khain, A., Rosenfeld, D., and Pokrovsky, A.: Aerosol impact on the dynamics and microphysics of deep convective clouds, Quart. J. Roy. Meteor. Soc., 131, 2639–2663,2005.
Khain, A., Rosenfeld, D., and Pokrovsky, A.: Simulation of aerosol effects on convective clouds developed under continental and maritime conditions, Geophys. Res. Abstracts, 5, 03180, European Geophysical Society, 2003.
Khain, A., BenMoshe, N., and Pokrovsky, A.: Factors determining the impact of aerosols on surface precipitation from clouds: Attempt of classification, J. Atmos. Sci., 65, 1721–1748, 2008.
Klemp, J. B., Skamarock, W. C., and Duddhia, J.: WRF Eulerian prototype model equations – height and mass vertical coordinates. Draft manuscript obtainable from http://www.mmm.ucar.edu/wrf/users/wrf-dyn-num.html, 2000.
Koch, D. and Rind, D.: Beryllium 10/beryllium 7 as a tracer of stratospheric transport, J. Geophys. Res., 103, 3907–3918, 1998.
Leaitch, W. R., Strapp, J. W., and Isaac, G. A.: Cloud droplet nucleation and cloud scavenging of aerosol sulfate in polluted atmosphere, Tellus, 38B, 328–344, 1986.
Lee, S. S., Donner, L. J., Phillips, V. T. J., and Ming, Y.: Examination of aerosol effects on precipitation in deep convective clouds during the 1997 ARM summer program, Quart. J. Roy. Meteor. Soc., in press, 2008a.
Lee, S. S., Donner, L. J., and Phillips, V. T. J., and Ming, Y.: The dependence of aerosol effects on clouds and precipitation on cloud-system organization, shear and stability, J. Geo-

phys. Res., in press, draft manuscript obtainable from http://www.agu.org/contents/journals/ViewPapersInPress.do?journalCode=JD, 2008b.
Liou, K. N.: Cirrus clouds and climate in McGraw-Hill Yearbook of Science and Technology, 432 pp., 2005.
Liou, K. N.: Influence of cirrus clouds on weather and climate processes: A global perspective, Mon. Wea. Rev., 114, 1167–1199, 1986.
Lynn, B. H., Khain, A. P., Dudhia, J., Rosenfeld, D., Pokrovsky, A. and Seifert, A.: Spectral (bin) microphysics coupled with a mesoscale model (MM5). Part I: Model description and first results, Mon. Wea. Rev., 133, 44–58, 2005.
Lohmann, U. and Diehl, K.: Sensitivity studies of the importance of dust ice nuclei for the indirect aerosol effect on stratiform mixed-phase clouds, J. Atmos. Sci., 63, 968–982, 2006.
Meyers, M. P., DeMott, P. J., and Cotton, W. R.: New primary ice-nulceation parameterization in an explicit cloud model, J. Appl. Meteor., 31, 708–720, 1992.
Michalakes, J., Chen, S., Dudhia, J., Hart, L., Klemp, J., Middlecoff, J., and Skamarock, W.: Development of a Next Generation Regional Weather Research and Forecast Model. Developments in Teracomputing: Proceedings of the Ninth ECMWF Workshop on t he Use of High Performance Computing in Meteorology Eds. Walter Zwieflhofer and Norbert Kreitz, World Scientific, Singapore, 269–276, 2001.
Ming, Y., Ramaswamy, V., Donner, L. J., and Phillips, V. T. J.: A new parameterization of cloud droplet activation applicable to general circulation models, J. Atmos. Sci., 63, 1348–1356, 2006.
Möhler, O., Field, P. R., Connolly, P., Benz, S., Saathoff, H., Schnaiter, M., Wagner, R., Cotton, R., Krämer, M., Mangold, A., and Heymsfield, A. J.: Efficiency of the deposition mode ice nucleation on mineral dust particles, Atmos. Chem. Phys., 6, 3007–3021, 2006, http://www.atmos-chem-phys.net/6/3007/2006/.
Phillips, V. T. J., Donner, L. J., and Garner, S.: Nucleation processes in deep convection simulated by a cloud-system-resolving model with double-moment bulk microphysics, J. Atrmos. Sci.,64, 738–761, 2007.
Ramanathan, V., Cess, R. D., Harrison, E. F., et al.: Cloud-Radiative Forcing and Climate: Results from the Earth Radiation Budget Experiment, Science, 243, 57–63, 1989.
Ramaswamy, V., Boucher, O., Haigh, J., et al.: Radiative forcing of climate change, in Climate Change 2001: The Scientific Basis, edited by: Houghton, J. T., Joos F., Srinivasan, J., et al., 349–416, Cambridge Univ. Press, New York, 2001.

Schwazkopf, M. D. and Ramaswamy, V.: Radiative effects of CH_4, N_2O, halocarbons and the foreign-broadened H_2O continuum: a GCM experiment. J. Geophys. Res., 104, 9467–9488, 1999.

Seinfeld, J. H. and Pandis, S. N.: Atmospheric chemistry and physics: From air pollution to climate change, John Wiley & Sons, 1326 pp., 1998.

Tao, W-K, Li, X., Khain, A., Matsui, T., Lang, S., Simpson, J.: The role of atmospheric aerosol concentration on deep convective precipitation: cloud-resolving model simulations, J. Geophys. Res., 112, D24S18, doi:10.1029/2007JD008728, 2007.

Timmreck C. and Schulz, M.: Significant dust simulation differences in nudged and climatological operation mode of the AGCM ECHAM, J. Geophys. Res., 109, D13202, doi:10.1029/2003JD004381, 2004.

Weisman, M. L. and Klemp, J. B.: The dependence of Numerically Simulated Convective Storms on Vertical Wind Shear and Buoyancy, Mon. Wea. Rev., 110, 504–520, 1982.

Whitby, K. T.: The physical characteristics of sulfur aerosols, Atmos. Environ., 12, 135–159, 1978.

Xu, K.-M., Cederwall, R. T., Donner, L. J., et al.: An intercomparison of cloud-resolving models with the Atmospheric Radiation Measurement summer 1997 Intensive Observation Period data, Quart. J. Roy. Meteor. Soc., 128, 593–624, 2002.

Young, K. C.: Microphysical processes in clouds, Oxford University Press, 427 pp, 1993.

Zhang, M. H., Lin, J. L., Cederwall, R. R., Yio, J. J., and Xie, S. C.: Objective analysis of ARM IOP data: method and sensitivity, Mon. Wea. Rev., 129, 295–311, 2001.

Table 1. Time- and area-averaged shortwave flux (SW) and longwave flux (LW) at the top (TOA) and base (SFC) of the atmosphere in DEEP. ↑ and ↓ denote upward and downward radiation, respectively.

Time- and area-averaged radiation fluxes at the top and base of the model (W m^{-2})														
TOA														
	SW↑		SW↓		SW (SW↑–SW↓)		LW↑		LW↓		LW (LW↑–LW↓)		SW+LW	
	ALL	CLR	ALL	CLR	ALL	CLR	ALL	CLR	ALL	CLR	ALL	CLR	ALL	CLR
Low aerosol	97.20	85.15	478.53	478.53	–381.33	–393.38	266.86	276.63	0.00	0.00	266.86	276.63	–114.47	–116.75
High aerosol	120.92	85.02	478.53	478.53	–357.61	–393.51	257.10	273.39	0.00	0.00	257.10	273.39	–100.51	–120.12
Observed	111.65	–	477.15	477.15	–365.50	–	260.23	–	0.00	0.00	260.23	–	–105.27	–
Difference (high–low)	23.72	–0.13	0.00	0.00	23.72	–0.13	–9.76	–3.24	0.00	0.00	–9.76	–3.24	13.96	–3.37
SFC														
	SW↑		SW↓		SW (SW↑–SW↓)		LW↑		LW↓		LW (LW↑–LW↓)		SW+LW	
	ALL	CLR	ALL	CLR	ALL	CLR	ALL	CLR	ALL	CLR	ALL	CLR	ALL	CLR
Low aerosol	60.43	70.63	316.53	371.57	–256.10	–300.94	442.10	442.10	365.61	361.85	76.49	80.25	–179.61	–220.69
High aerosol	55.56	70.60	288.07	370.67	–232.51	–300.07	442.10	442.10	370.17	362.16	71.93	79.94	–160.58	–220.13
Observed	54.64	–	279.44	–	–224.80	–	453.99	–	397.12	–	56.87	–	–167.93	–
Difference (high–low)	–4.87	–0.03	–28.46	–0.90	23.59	0.87	0.00	0.00	4.56	0.31	–4.56	–0.31	19.03	0.56

ACPD
8, 15291–15341, 2008

Table 2. Time- and area-averaged SW and LW at the top (TOA) and base (SFC) of the atmosphere in SHALLOW.

Time- and area-averaged radiation fluxes at the top and base of the model (W m^{-2})														
TOA														
	SW↑		SW↓		SW (SW↑–SW↓)		LW↑		LW↓		LW (LW↑–LW↓)		SW+LW	
	ALL	CLR	ALL	CLR	ALL	CLR	ALL	CLR	ALL	CLR	ALL	CLR	ALL	CLR
Low aerosol	93.11	38.24	478.53	478.53	–385.42	–440.29	274.26	283.25	0.00	0.00	274.26	283.25	–111.16	–157.04
High aerosol	111.21	38.12	478.53	478.53	–367.32	–440.41	273.46	282.90	0.00	0.00	273.46	282.90	–93.86	–157.51
Observed	–	–	–	–	–	–	–	–	–	–	–	–	–	–
Difference (high–low)	18.10	–0.12	0.00	0.00	18.10	–0.12	–0.80	–0.35	0.00	0.00	–0.80	–0.35	17.30	–0.47
SFC														
	SW↑		SW↓		SW (SW↑–SW↓)		LW↑		LW↓		LW (LW↑–LW↓)		SW+LW	
	ALL	CLR	ALL	CLR	ALL	CLR	ALL	CLR	ALL	CLR	ALL	CLR	ALL	CLR
Low aerosol	23.92	27.02	319.62	374.75	–295.70	–347.73	424.60	424.60	356.69	350.35	67.91	74.25	–227.79	–273.48
High aerosol	21.32	26.73	298.19	373.89	–276.87	–347.16	425.14	425.14	357.76	350.02	67.38	75.12	–209.49	–272.04
Observed	–	–	–	–	–	–	–	–	–	–	–	–	–	–
Difference (high–low)	–2.60	–0.29	–21.43	–0.86	18.83	0.57	0.54	0.54	1.07	–0.33	–0.53	0.87	18.30	1.44

ACPD
8, 15291–15341, 2008

Table 3. Time- and area-averaged TOA and SFC shortwave cloud forcing (SCF), longwave cloud forcing (LCF), and cloud radiative forcing (CRF) (W m^{-2}), i.e. SCF+LCF, for DEEP, SHALLOW and DEEP (LIQ).

TOA (W m^{-2})									
	SCF			LCF			CRF		
	DEEP	SHALLOW	DEEP (LIQ)	DEEP	SHALLOW	DEEP (LIQ)	DEEP	SHALLOW	DEEP (LIQ)
Low aerosol	–12.05	–54.87	–4.97	9.77	8.99	2.11	–2.28	–45.88	–2.86
High aerosol	–35.90	–73.09	–18.08	16.29	9.44	4.52	–19.61	–63.65	–13.56
Difference (high–low)	–23.85	–18.22	–13.11	6.52	0.45	2.41	–17.33	–17.77	–10.70
SFC (W m^{-2})									
	SCF			LCF			CRF		
	DEEP	SHALLOW	DEEP (LIQ)	DEEP	SHALLOW	DEEP (LIQ)	DEEP	SHALLOW	DEEP (LIQ)
Low aerosol	–44.84	–52.03	–10.24	3.76	6.34	0.88	–41.08	–45.69	–9.36
High aerosol	–67.56	–70.29	–21.38	8.01	7.74	2.64	–59.55	–62.55	–18.74
Difference (high–low)	–22.72	–18.26	–11.14	4.25	1.40	1.76	–18.47	–16.86	–9.38

ACPD
8, 15291–15341, 2008

Table 4. Time- and area-averaged TOA SCF, LCF, and CRF (W m^{-2}) for SHALLOW (IDEAL), DEEP (CU) and DEEP (LOW-CU).

	TOA (W m^{-2})								
	SCF			LCF			CRF		
	SHALL OW (IDEAL)	DEEP (CU)	DEEP (LOW-CU)	SHALLOW (IDEAL)	DEEP (CU)	DEEP (LOW-CU)	SHALLOW (IDEAL)	DEEP (CU)	DEEP (LOW-CU)
Low aerosol	–20.21	–15.43	–25.02	3.64	5.24	6.26	–16.57	–10.19	–18.76
High aerosol	–40.01	–39.45	–43.79	4.60	10.65	9.63	–35.41	–28.80	–34.16
Difference (high–low)	–19.80	–24.02	–18.77	0.96	5.41	3.37	–18.84	–18.61	–15.40

ACPD
8, 15291–15341, 2008

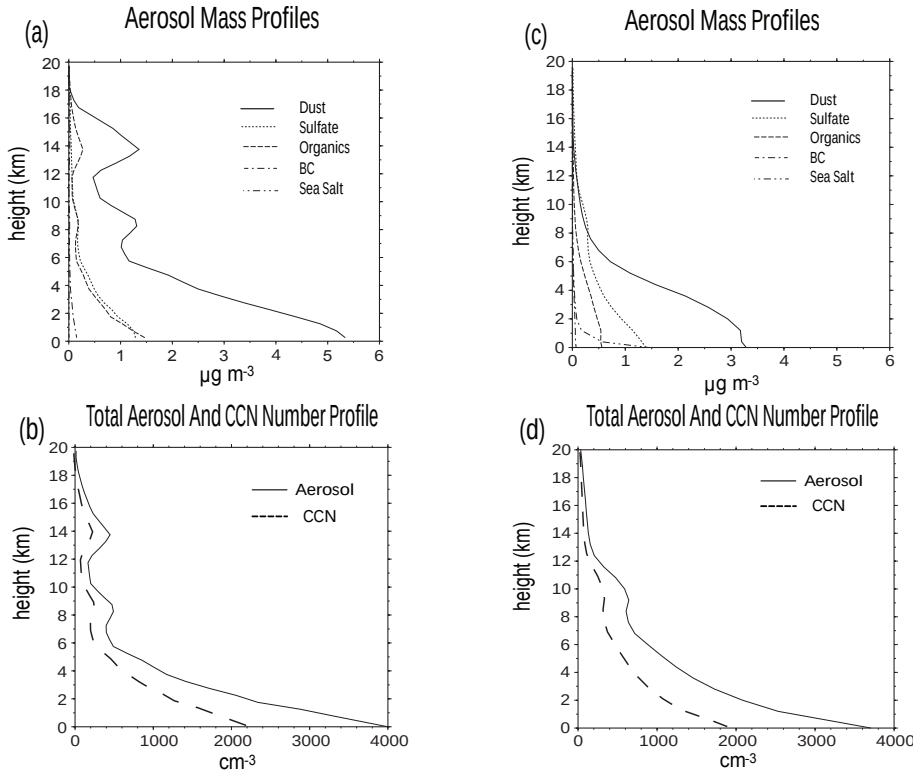

Fig. 1. Vertical profiles of **(a)** aerosol species and **(b)** total aerosol number and CCN number (at supersaturation of 1%) for high aerosol runs in DEEP. Salt is present in (a), but its values are less than 0.01 $\mu g\,m^{-3}$. **(c)** and **(d)** are the same as (a) and (b), respectively, but for SHALLOW.

ACPD
8, 15291–15341, 2008

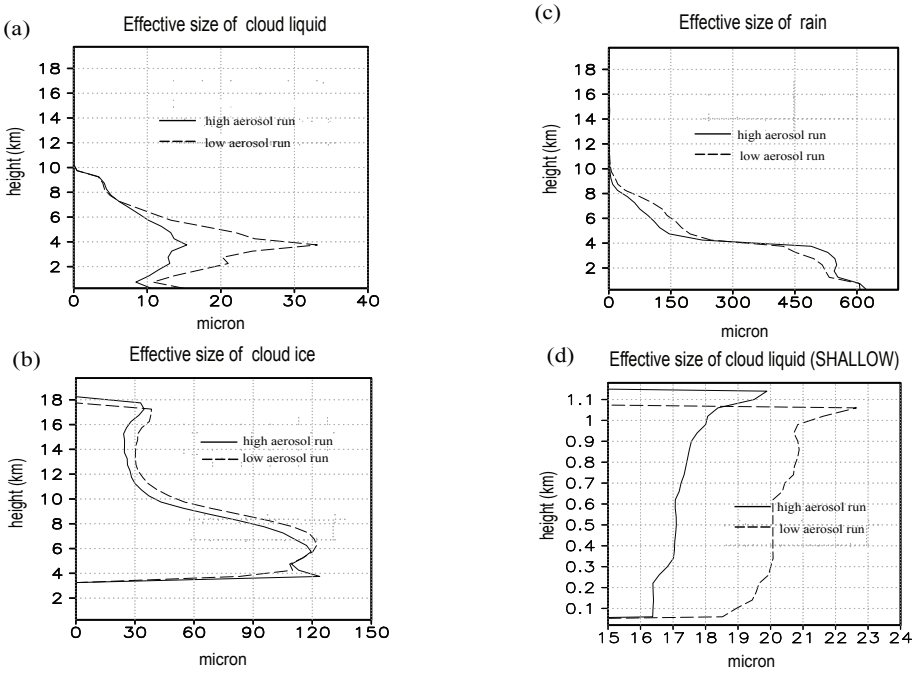

Fig. 2. Vertical distribution of in-cloud average effective size of **(a)** cloud liquid, **(b)** cloud ice and **(c)** rain in DEEP. **(d)** is the same as (a) but for SHALLOW.

ACPD
8, 15291–15341, 2008

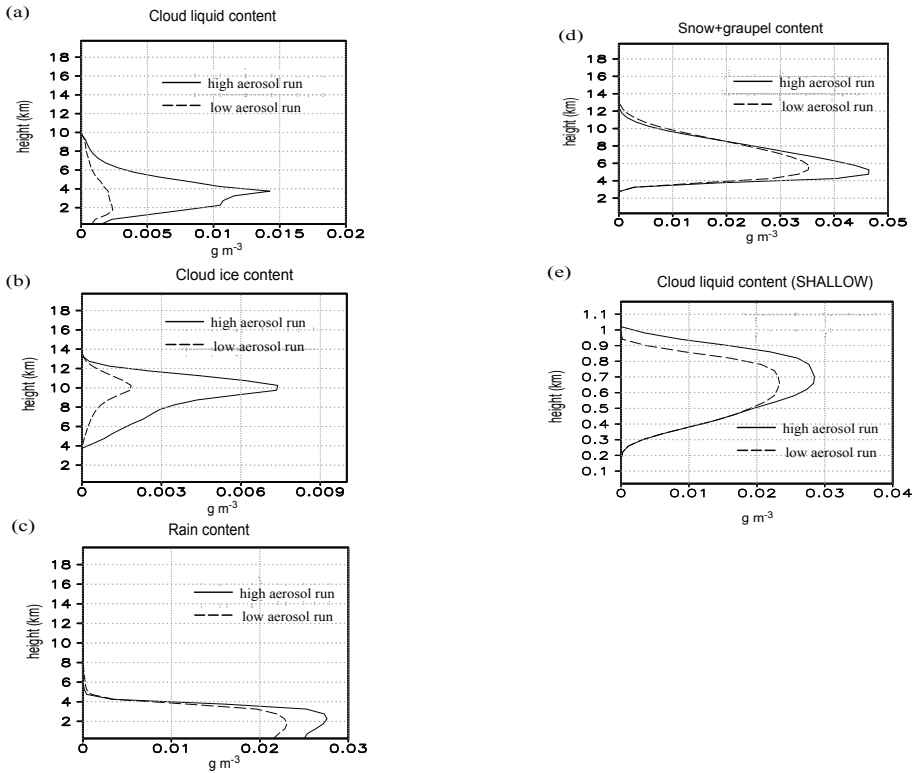

Fig. 3. Time- and domain-averaged vertical distribution of contents of **(a)** cloud liquid, **(b)** cloud ice, **(c)** rain and **(d)** snow+graupel. **(e)** is the same as (a) but for SHALLOW.

ACPD
8, 15291–15341, 2008

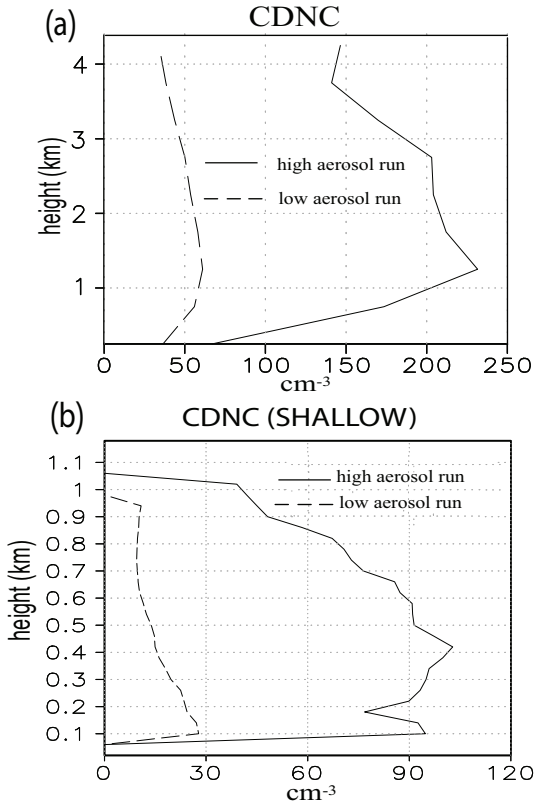

Fig. 4. Vertical distribution of in-cloud average CDNC (cm^{-3}) **(a)** in DEEP and **(b)** in SHALLOW, conditionally averaged over grid points of non-zero droplet nucleation rate below freezing level.

ACPD
8, 15291–15341, 2008

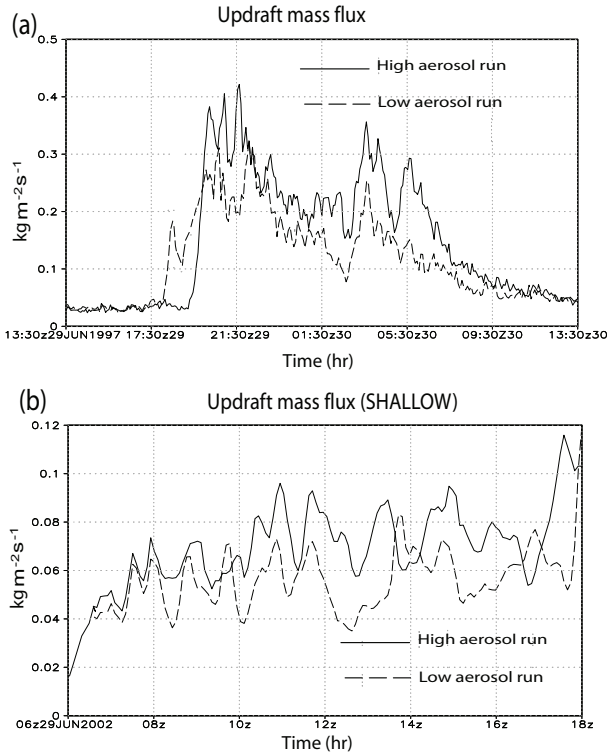

Fig. 5. Time series of domain-averaged updraft mass flux (for those whose values are above-zero) **(a)** in DEEP at the lowest 5 km and **(b)** in SHALLOW at the lowest 1.5 km.

ACPD
8, 15291–15341, 2008

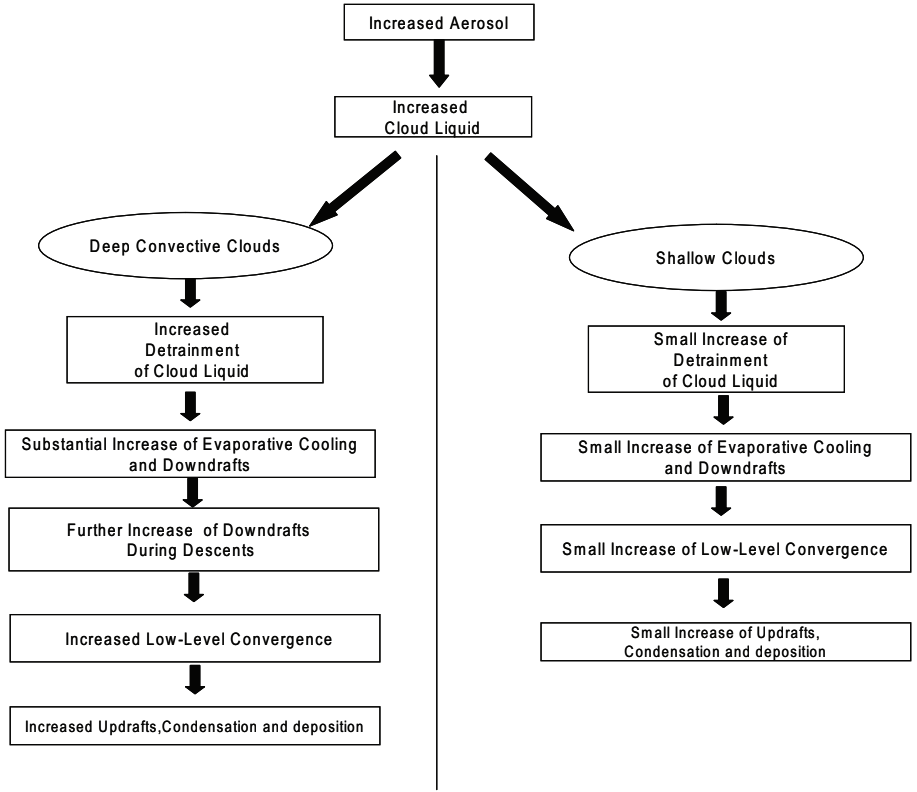

Fig. 6. Schematic diagram illustrating the differing extent of interactions between aerosols, microphysics, and dynamics in deep and shallow convection.

ACPD
8, 15291–15341, 2008

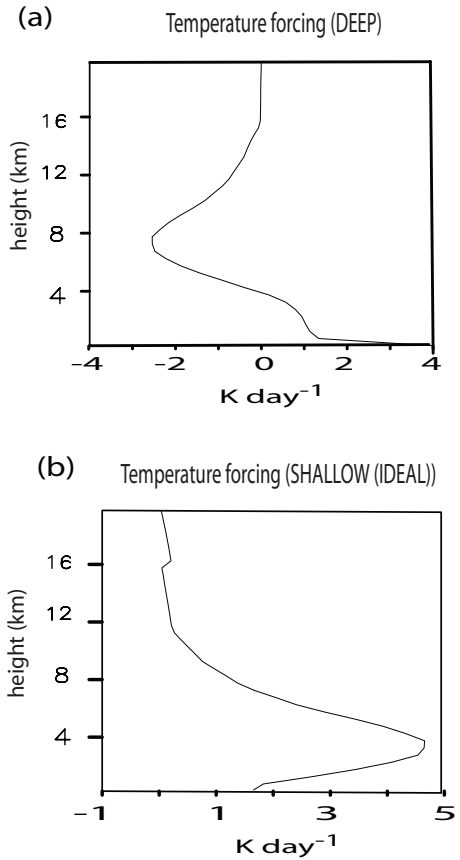

Fig. 7. Time- and domain-averaged vertical distribution of potential temperature large-scale forcing (K day^{-1}) for **(a)** DEEP and **(b)** SHALLOW (IDEAL).

ACPD
8, 15291–15341, 2008

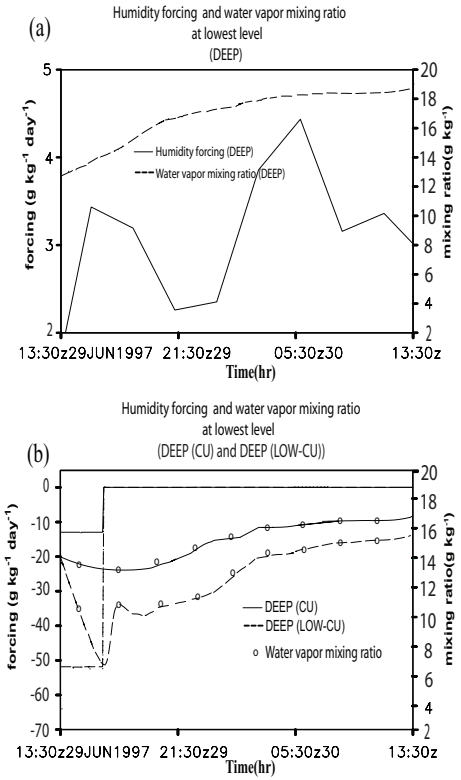

Fig. 8. Time series of humidity large-scale forcing and area-averaged water vapor mixing ratio at the lowest level of the atmosphere **(a)** for DEEP and **(b)** for DEEP (CU) and DEEP (LOW-CU).

ACPD
8, 15291–15341, 2008

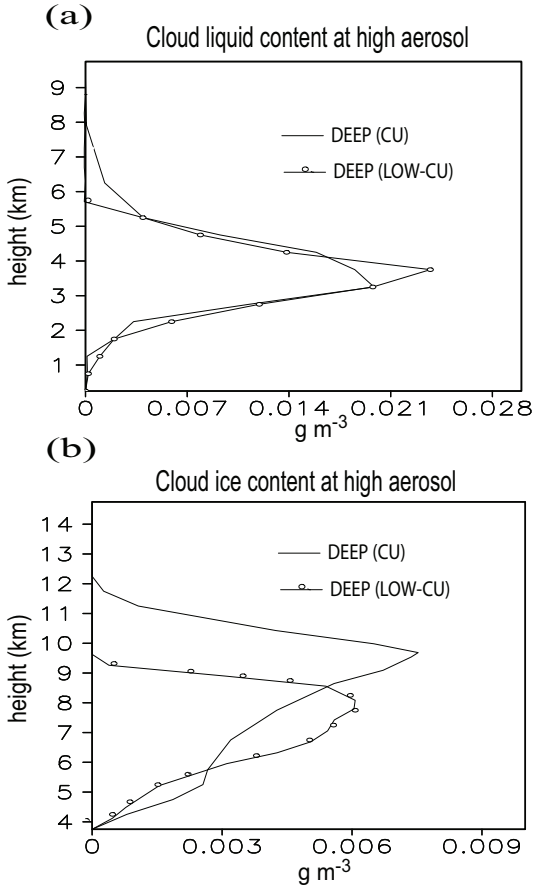

Fig. 9. Vertical profiles of time- and domain-averaged contents of **(a)** cloud liquid and **(b)** cloud ice in the high-aerosol runs for DEEP (CU) and DEEP (LOW-CU).

ACPD
8, 15291–15341, 2008

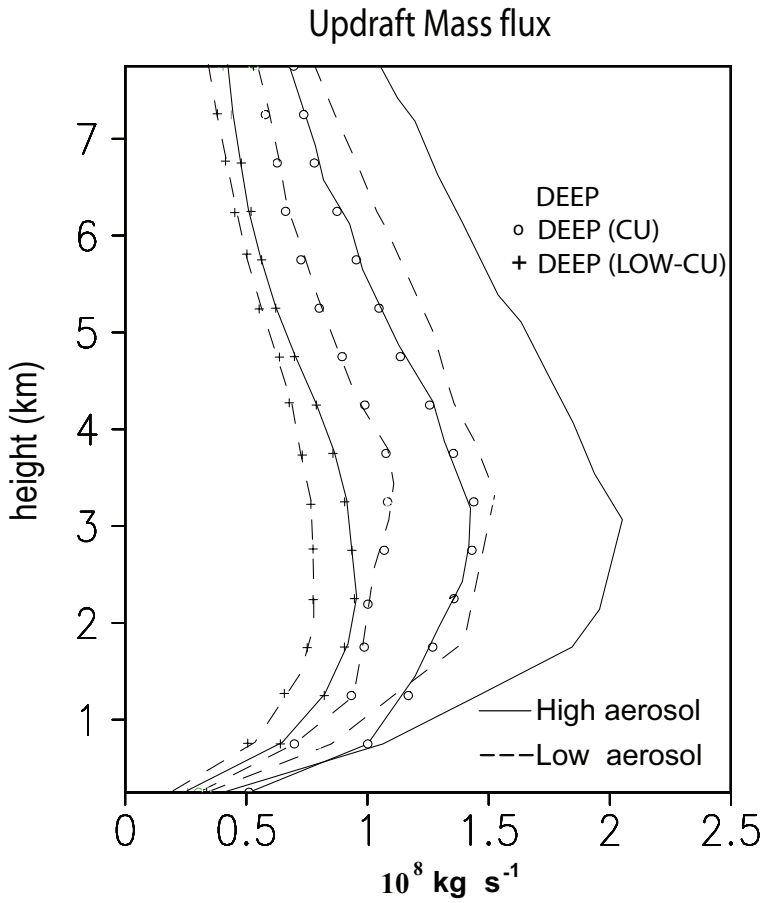

Fig. 10. Vertical profiles of time-averaged updraft mass flux (for those whose values are above-zero) for DEEP, DEEP (CU) and DEEP (LOW-CU).

ACPD
8, 15291–15341, 2008